Analysis of bifurcations in multiharmonic analysis of nonlinear forced vibrations of gas-turbine engine structures with friction and gaps

Article (Published Version)

Proceedings of ASME Turbo Expo 2015: Turbine Technical Conference and Exposition
GT2015
June 15 – 19, 2015, Montréal, Canada

GT2015-43670

ANALYSIS OF BIFURCATIONS IN MULTIHARMONIC ANALYSIS OF NONLINEAR FORCED VIBRATIONS OF GAS-TURBINE ENGINE STRUCTURES WITH FRICTION AND GAPS

E.P. Petrov

University of Sussex, School of Engineering and Informatics,
Brighton BN1 9QT, United Kingdom, Email: y.petrov@sussex.ac.uk

ABSTRACT

An efficient frequency-domain method has been developed to analyse the forced response of large-scale nonlinear gas-turbine structures with bifurcations. The method allows: detection and localization of the design and operating conditions sets where bifurcations occur; calculation of tangents to the solution trajectory and continuation of solutions under parameter variation for structures with bifurcations.

The method is aimed at calculation of steady-state periodic solution and multiharmonic representation of the variation of displacements in time is used. The possibility of bifurcations in realistic gas-turbine structures with friction contacts and with cubic nonlinearity has been shown.

INTRODUCTION

Gas turbine engines and their major components, such as bladed discs with dampers and/or root joints, rotors on squeeze-film or magnetic bearings, casing with flanges and other types of joints, whole engine models are generally nonlinear structures. The nonlinear interactions are usually localised at contact interfaces between assembled components (e.g. at blade-disc root joints or at damper contact surfaces), or at location where high energy rubbing contacts occurs (e.g. as a result of rubbing contact of rotor blades and casing). The nonlinear contact interaction forces are usually due to friction, closing and opening gaps, variable contact areas, devices and supports with inherently nonlinear characteristics. The accurate prediction of strongly nonlinear behaviour requires using large-scale finite element models for all interacting components and high-fidelity modelling for the nonlinear contact interface interactions.

Development of methods for analysis and numerical studies of nonlinear vibration in gas turbine engines become a major interest for the industry and attracts efforts of many researchers (e.g. see Refs. [1]-[8]). In most recent studies the steady-state vibrations are analysed in frequency domain and are based on the harmonic balance methods, although some formulations (Refs.[9] and [10]) require a restricted part of the analysis to be performed in time domain. The analysis can be performed to find forced response amplitudes, to calculate directly resonance peak amplitudes (Ref. [11]) together with their sensitivity to design parameters (Refs. [12] and [13]). There are significant number of monographs and papers considering bifurcation analysis for of dynamic structures (e.g. see Refs.[14] - [18]). However, one major phenomenon – bifurcation – has not been addressed and studied for complex gas-turbine structures and, moreover, for a general case of multiharmonic analysis of strongly nonlinear structures in the frequency domain.

The phenomenon of bifurcation of nonlinear forced response vibrations can be observed in such nonlinear structures when, even under smooth variation of operating conditions, for some set of structural parameters and excitation several different steady-state vibration regimes can occur and, moreover, the vibration regime can change abruptly its qualitative properties.

The analysis of bifurcations represents a challenging and under-investigated problem of high practical importance.

In the proposed paper, a methodology is developed for frequency domain analysis of bifurcations of nonlinear steady-state forced response vibration in gas-turbine engine structures and turbomachines with friction, gap and rubbing contact interfaces. The methodology allows using large-scale finite element models for structural components together with detailed and high-fidelity description of non-smooth nonlinear interactions at contact interfaces between these components. The method solves in frequency domain all major problems of the

bifurcation analysis: (i) detection of the bifurcation points; (ii) exact localisation of the bifurcation point, (iii) calculation of all possible vibration regimes emanating from the bifurcation point and (iv) tracing of all bifurcating vibration regimes under operating or structural parameter variation: e.g. rotation speed, gap or friction coefficient values.

Analysis of bifurcations in structures with rubbing rotor-stator friction contacts has been performed for: (i) a simplified rotor on nonlinear supports and (ii) for a realistic whole engine model comprising flexible finite element models of realistic engine rotor and casing. High accuracy and computational efficiency of the methodology is demonstrated. Validation of the results obtained by the new methods is performed by comparison with the results of direct integration of equations of motion obtained by analysis performed in time domain.

BIFURCATIONS IN FREQUENCY-DOMAIN FORCED RESPONSE ANALYSIS

The equation of motion for the forced vibrations of a structure with nonlinear contact interfaces takes the form:

$$\boldsymbol{K}\boldsymbol{x}+\boldsymbol{C}\dot{\boldsymbol{x}}+\boldsymbol{M}\ddot{\boldsymbol{x}}+\boldsymbol{f}(\boldsymbol{x},\dot{\boldsymbol{x}})=\boldsymbol{p}(t) \qquad (1)$$

where $\boldsymbol{x}(t)$ is a vector of displacements for all degrees of freedom (DOFs) in the structure considered; $\boldsymbol{K}$, $\boldsymbol{C}$ and $\boldsymbol{M}$ are structural stiffness, damping and mass matrices of finite element (FE) model of a structure. For bladed discs and other structures mounted on a rotating rotor, the stiffness matrix can include terms accounting for the rotation effects (e.g. Coriolis forces, gyroscopic moments, rotation stiffening effects) and, therefore, is generally dependent on the rotation speed, Ω. $\boldsymbol{p}(t)$ is a vector of excitation forces and $\boldsymbol{f}(\boldsymbol{x},\dot{\boldsymbol{x}})$ is a vector of nonlinear contact interface forces. The contact forces occur in gas-turbine structures at the blade root joints of bladed discs, at contact surfaces of underplatform or tip dampers, at contact surfaces of adjacent interlock shrouds and at rubbing contacts between rotor and casing. The causes of nonlinear behaviour are usually friction forces, unilateral interaction at the pairing contact surfaces, gaps, varying contact stiffness properties, as in the case of Hertzian contacts, etc. In this paper, a case of periodic excitation forces is considered: $\boldsymbol{p}(t)=\boldsymbol{p}(t+2\pi/\omega)$, where ω is the principal excitation frequency and the steady-state periodic oscillations are studied. A general case is studied here, when the principal excitation frequency may not be related to the rotation speed, Ω, although for the majority of dynamic problems in gas-turbine engines the principal excitation frequency is equal or multiple of the rotation speed: $\omega=k\Omega\ (k=1,2,...)$.

The time variation of displacements and the nonlinear contact forces for the steady-state periodic regimes is represented by a restricted Fourier series:

$$\boldsymbol{x}(t)=\boldsymbol{X}_0+\sum_{j=1}^{n}\left(\boldsymbol{X}_j^{(c)}\cos m_j\omega t+\boldsymbol{X}_j^{(s)}\sin m_j\omega t\right) \qquad (2)$$

$$\boldsymbol{f}(\boldsymbol{x},\dot{\boldsymbol{x}})=\boldsymbol{F}_0^{(c)}+\sum_{j=1}^{n}\left(\boldsymbol{F}_j^{(c)}\cos m_j\omega t+\boldsymbol{F}_j^{(s)}\sin m_j\omega t\right) \qquad (3)$$

The harmonic numbers, m_j, and their total number, n, are chosen to provide sufficiently accurate description of the periodic motion calculated. For a case when major and superharmonic vibrations are calculated (and the vibration period is equal or smaller than the excitation frequency), the harmonic numbers, m_j, are integer numbers. For a case when subharmonic vibrations have to be analysed, some of the harmonic numbers can be represented by fractional numbers which provide the possibility to calculate periodic nonlinear responses with the vibration period larger than the period of the excitation forces.

The application of the harmonic balance method together with the expressions for the dependency of the nonlinear contact on displacements as described in Ref.[3] provides the nonlinear frequency-domain equation of motion:

$$\boldsymbol{R}(\boldsymbol{X},\lambda)=\boldsymbol{X}+\boldsymbol{A}(\lambda_A)\left(\boldsymbol{F}(\boldsymbol{X},\lambda_F)-\boldsymbol{P}(\lambda_P)\right)=\boldsymbol{0} \qquad (4)$$

where $\boldsymbol{X}$ and $\boldsymbol{F}$ are vectors of harmonic coefficients for displacements and contact forces; $\boldsymbol{P}$ is the vector of harmonic coefficients for the excitation forces, $\boldsymbol{A}$ is the frequency response function (FRF) matrix and λ_A, λ_F and λ_P are some parameters of the structure, contact interfaces or excitation forces accordingly. For example, λ_A can be the principal excitation frequency (i.e. $\lambda_A=\omega$), modal damping factor or natural frequency value; λ_F can be some parameter of the contact interfaces, such as friction coefficient, gap or interference value, contact stiffness coefficient, the principal frequency, etc.; λ_P can be the excitation level for each harmonic component of the excitation forces or the principal frequency.

The solution of Eq.(4) is usually required to be calculated not for one set of the design parameters but in some range of parameters characterising the structure, nonlinear contact interfaces, excitation frequency, excitation levels, etc. Therefore, each of the parameters in Eq.(4) can be chosen as a so-called tracing or continuation parameter (i.e. $\lambda=\lambda_A$, λ_F or λ_P) to obtain solutions of this nonlinear equation for all possible values of the chosen parameter. Moreover, all parameters can be varied simultaneously with prescribed functions of the variation of physical parameters: $\lambda_A(\lambda)$, $\lambda_F(\lambda)$ and $\lambda_P(\lambda)$. The solution of the nonlinear equation of motion can be efficiently performed using so-called solution continuation methods (Refs.[19] - [21]) and the multiharmonic displacements are determined as a function of the continuation parameter: $\boldsymbol{X}=\boldsymbol{X}(\lambda)$.

For strongly nonlinear vibrations, for certain values of the parameters, the number of possible solutions can abruptly change and new solutions emerge at the point corresponding to this special set of the design and operating condition parameters. The points on the trajectory of solutions at which the new solutions emanate are called bifurcation points. The bifurcation points are called also branching points since the new branches of solutions emanate at these points of the solution trajectory. An example of a solution trajectory with a bifurcation point is given

in **Fig. 1** where in addition to the original trajectory of solution (shown in black) two new solution branches emerge at the bifurcation point.

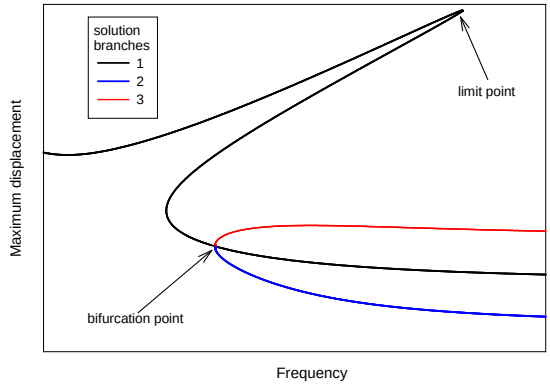

Fig. 1 A trajectory of maximum displacement calculated as a function of excitation frequency

The analysis of bifurcations has large practical importance since, in the presence of bifurcations, any of the branching solutions emanating from a bifurcation point, can be realised and different vibration regimes can occur for the same operating conditions. The possibility of the occurrence of such different vibratory regimes need to be accounted for in the design process. The realisation of one or another regime is usually dependent on the initial values of the nodal displacements and velocities at which the structure comes to the operating conditions of interest, where the steady-state response has to be determined. The initial conditions are dependent on the history of the gas-turbine engine operation including possible abrupt random perturbations and impacts.

Moreover, the determination of the bifurcation points is necessary to ensure an efficient numerical procedure for tracing of the solution under the parameter variation since at the bifurcation points the standard continuation algorithms Refs.[19] - [21]) can fail. Usually it is exhibited in the infinite loops around a bifurcation point or in the forced re-direction of the tracing process backward to follow the solution branch which is already calculated. In some cases the tracing of solutions can be successfully performed, but, without a special method for dealing with the bifurcations, only one solution branch can be determined while the other solutions emanating at the bifurcation points are missed and, therefore, completely ignored in the design process.

A method developed here for efficient tracing the nonlinear multiharmonic forced response solutions for structures with bifurcations includes the following major constituents:

1) the detection of the bifurcation points during the solution tracing;
2) the localisation of the bifurcation points, i.e. obtaining accurate values of parameters when the bifurcation occurs;
3) the calculation of the tangents to the branching solutions;
4) the tracing of branching solutions emanating from the found bifurcation points.

The details of the implementation of the method for each of these constituents are discussed in the following sections.

DETECTION OF THE BIFURCATION POINTS DURING SOLUTION TRACING

The dependency of the nonlinear solution on the design parameters values can be complex. In the presence of multitude possible solutions corresponding to the same design parameters, to ensure that one selected solution trajectory is calculated the nonlinear frequency-domain Eq. (4) is supplemented by an additional equation and the following equation is solved:

$$\boldsymbol{R}_1(\boldsymbol{X},\lambda)=\begin{Bmatrix}\boldsymbol{R}(\boldsymbol{X},\lambda)\\ r_1(\boldsymbol{X},\lambda)\end{Bmatrix}=\boldsymbol{0} \tag{5}$$

The additional, tracing equation, $r_1(\boldsymbol{X},\lambda)=0$, provides uniqueness of the solution for all points at the trajectory of solutions (except of the bifurcation points). It can take different forms, for example, in the well-known arc-length continuation (e.g. see Ref.[20]), it takes the form:

$$r_1(\boldsymbol{X},\lambda)=\left\|\left(\boldsymbol{X}-\boldsymbol{X}_*\right)\right\|^2+\left(\lambda-\lambda_*\right)^2-\delta s^2 \tag{6}$$

where δs is step length along the trajectory of the solution; $\boldsymbol{X}_*$ and λ_* are values of multiharmonic displacements and design parameter already calculated at the previous step. Examples of other tracing equations can be found in Refs.[19] and [21].

During the tracing process, the solutions are calculated at discrete points along the solution trajectory, choice of the step length is selected automatically to ensure sufficiently fast convergence of the solution process and to capture the details of the solution trajectory. Each solution tracing step is based on the prediction of the solution and then its correction is performed to obtain its exact values.

At the prediction stage, an approximation to the solution $\left(\boldsymbol{X}_0,\lambda_0\right)$ is calculated using the tangent to the trajectory of the solution calculated at the solution point, $\boldsymbol{t}=\left\{\boldsymbol{t}_x,t_\lambda\right\}^T$:

$$\boldsymbol{X}_0=\boldsymbol{X}_*+\boldsymbol{t}_x\delta s\quad \lambda_0=\lambda_*+t_\lambda\delta s \tag{7}$$

At the correction stage the iterative Newton-Raphson algorithm is applied, which allows calculation of the solution with any desired accuracy:

$$\begin{bmatrix}\boldsymbol{J} & \boldsymbol{R}_\lambda\\ \dfrac{\partial r_1}{\partial \boldsymbol{X}} & \dfrac{\partial r_1}{\partial \lambda}\end{bmatrix}\begin{Bmatrix}\delta\boldsymbol{X}\\ \delta\lambda\end{Bmatrix}=\boldsymbol{J}_1\left(\boldsymbol{X}_j,\lambda_j\right)\begin{Bmatrix}\delta\boldsymbol{X}\\ \delta\lambda\end{Bmatrix}=-\begin{Bmatrix}\boldsymbol{R}\left(\boldsymbol{X}_j,\lambda_j\right)\\ r_1\left(\boldsymbol{X}_j,\lambda_j\right)\end{Bmatrix} \tag{8}$$

$$\boldsymbol{X}_{j+1}=\boldsymbol{X}_j+\delta\boldsymbol{X};\quad \lambda_{j+1}=\lambda_j+\delta\lambda;\quad j=0,1,2,... \tag{9}$$

where $\boldsymbol{J}=\partial\boldsymbol{R}/\partial\boldsymbol{X}=\boldsymbol{I}+\boldsymbol{A}\boldsymbol{K}$; $\boldsymbol{I}$ is the identity matrix; $\boldsymbol{K}=\partial\boldsymbol{F}/\partial\boldsymbol{X}$ is nonlinear contact stiffness matrix; $\boldsymbol{R}_\lambda=\partial\boldsymbol{R}/\partial\lambda$ and subscripts j and $j+1$ correspond to the iteration number. The iterative calculation is finished when the required accuracy is achieved and at the found new solution, $\left(\boldsymbol{X}_*,\lambda_*\right)$, a tangent to the solution trajectory is calculated from the following equation:

$$\left[\boldsymbol{J}\left(\boldsymbol{X}_*,\lambda_*\right)\middle|\boldsymbol{R}_\lambda\left(\boldsymbol{X}_*,\lambda_*\right)\right]\begin{Bmatrix}\boldsymbol{t}_x\\ t_\lambda\end{Bmatrix}=\boldsymbol{0} \tag{10}$$

The classification of the found solution can be easily made using the values of the determinants of Jacobians for Eq.(4) and Eq.(5):

- a bifurcation point if:

$$\det(\boldsymbol{J}) = 0 \quad \text{and} \quad \det(\boldsymbol{J}_1) = 0 \tag{11}$$

- a limit (turning) point (see **Fig. 1**) if:

$$\det(\boldsymbol{J}) = 0 \quad \text{and} \quad \det(\boldsymbol{J}_1) \neq 0 \tag{12}$$

- a regular point if:

$$\det(\boldsymbol{J}) \neq 0 \quad \text{and} \quad \det(\boldsymbol{J}_1) \neq 0 \tag{13}$$

Therefore, if signs for $\det(\boldsymbol{J}_1)$ at two adjacent solutions differ then there is a bifurcation point and it is located between these solutions. The change of sign for $\det(\boldsymbol{J}_1)$ is a sufficient condition for the bifurcation point, although it is not a necessary condition for bifurcation point detection, since $\det(\boldsymbol{J}_1)$ can achieve zero values in some cases without changing its sign.

For considered in this paper so-called 'simple bifurcations' where two solution curves intersect at a bifurcation point the change of sign of $\det(\boldsymbol{J}_1)$ is a good indicator of the bifurcation. The determinant, $\det(\boldsymbol{J}_1)$, of the Jacobian for Eq.(5), can be calculated without any significant computations efforts, practically as a by-product of the Newton-Raphson iterations (Eq.(8)). The expression for efficient evaluation of this determinant can be written in the form:

$$\det(\boldsymbol{J}_1) = \det(\boldsymbol{J})\left(\frac{\partial r_1}{\partial \lambda} + t_\lambda^{-1}\frac{\partial r_1}{\partial \boldsymbol{X}}\boldsymbol{t}_x\right) \tag{14}$$

LOCALISATION OF THE BIFURCATION POINT

Branching point equation

To determine accurately the solution corresponding to the bifurcation point we have to formulate an equation which would include the original equation of motion (Eq.(4)) and the bifurcation condition (Eq.(11)). In order to be able to calculate analytically the Jacobian of the branching equation we, following to ideas suggested in Ref. [15] for turning points and extended in Ref.[16] for bifurcation points, will use the condition that Jacobian has no-zero null space, instead of using the condition that the determinant of the Jacobian is zero. The equation for determination of the bifurcation point takes the form:

$$\boldsymbol{R}_2(\boldsymbol{X},\lambda,\boldsymbol{h},\gamma) = \begin{Bmatrix} \boldsymbol{R}(\boldsymbol{X},\lambda) + \gamma\boldsymbol{e}_j \\ \boldsymbol{J}(\boldsymbol{X},\lambda)\boldsymbol{h} \\ r_2(\boldsymbol{h}) \\ \boldsymbol{R}_\lambda^T(\boldsymbol{X},\lambda)\boldsymbol{h} \end{Bmatrix} = \boldsymbol{0} \tag{15}$$

Here $\boldsymbol{h}$ is an auxiliary vector belonging to the Jacobian null space; $r_2(\boldsymbol{h}) = \|\boldsymbol{h}\|^2 - 1$ is the condition that this vector is not zero; $\boldsymbol{e}_j$ is a unit vector with j-th component equal to 1 (where j is the number of a position with the maximum absolute value in the vector of initial approximation for vector $\boldsymbol{h}$); and γ is an auxiliary variable introduced here to have the Jacobian of Eq.(15) non-singular. The formula for Newton-Raphson iterations performed for the solution of Eq.(15) takes the following form:

$$\begin{bmatrix} \boldsymbol{J} & \boldsymbol{0} & \boldsymbol{R}_\lambda & \boldsymbol{e}_j \\ \partial(\boldsymbol{J}\boldsymbol{h})/\partial\boldsymbol{X} & \boldsymbol{J} & \partial(\boldsymbol{J}\boldsymbol{h})/\partial\lambda & \boldsymbol{0} \\ \boldsymbol{0} & 2\boldsymbol{h}^T & 0 & 0 \\ \boldsymbol{0} & \boldsymbol{R}_\lambda^T & 0 & 0 \end{bmatrix} \begin{Bmatrix} \delta\boldsymbol{X} \\ \delta\boldsymbol{h} \\ \delta\lambda \\ \delta\gamma \end{Bmatrix} = -\begin{Bmatrix} \boldsymbol{R} + \gamma\boldsymbol{e}_j \\ \boldsymbol{J}\boldsymbol{h} \\ r_2 \\ \boldsymbol{R}_\lambda^T\boldsymbol{h} \end{Bmatrix} \tag{16}$$

Choice of the solution approximation

The convergence rate and even the ultimate success or failure in the calculation of the branching point is dependent significantly on the choice of the initial approximation for all unknowns involved in Eq.(15). The approaches suggested here are based on our experience obtained in the analysis of rather wide examples of test cases and realistic models of gas-turbine engine structures.

First we need to find the initial approximation for the displacements, $\boldsymbol{X}$, and tracing parameters, λ. From the solution tracing we know two solution points between which the bifurcation point is located and, in many cases, the choice from these solutions that solution which provides smaller value for $\det(\boldsymbol{J}_1)$ can be a good initial approximation. Yet, to ensure sufficient closeness of the initial approximation to the bifurcation point in all cases the interval comprising the bifurcation point is usually traced with the reduced step size and then the solution closest to the bifurcation point, $\left(\tilde{\boldsymbol{X}}_0, \tilde{\lambda}_0\right)$, is chosen as the initial approximation. Next, the approximation for the null vector, $\boldsymbol{h}$, of Jacobian, $\boldsymbol{J}\left(\tilde{\boldsymbol{X}}_0, \tilde{\lambda}_0\right)$ is calculated by performing the singular value decomposition of the Jacobian and selecting from right-hand eigenvectors a vector corresponding to the minimum magnitude of the singular value. For the auxiliary variable, γ, the initial value is assumed to be 0.

Solution of the branching equation

The size of the mutliharmonic equation of motion is usually large, when realistic models of gas-turbine structures are analysed and the number of degrees of freedom (DOFs) at contact interfaces and the total number of harmonics used in the multiharmonic expansion are significant. Therefore, the direct solution of Eq.(16) is not only inefficient but in most cases practically impossible. Moreover, the additional difficulty for the solution process occurs here due to the fact that the Jacobian, $\boldsymbol{J}$, becomes singular at the bifurcation point. To deal with the Jacobian singularity a regularised matrix (Ref.[18]) is introduced:

$$\boldsymbol{J}_\alpha = \boldsymbol{J} + \alpha\boldsymbol{e}_j\boldsymbol{e}_j^T \tag{17}$$

where α is a coefficient chosen here as an average of all diagonal elements of matrix $\boldsymbol{J}$ taken by their absolute values, and j corresponds to the location of the minimum diagonal element.

Now we will solve Eq.(16) analytically. First, we re-write first line of Eq.(16) in the form:

$$\boldsymbol{J}_\alpha \delta\boldsymbol{X} = \left(-\boldsymbol{R} - \boldsymbol{e}_j \delta\gamma\right) - \boldsymbol{R}_\lambda \delta\lambda - \boldsymbol{e}_j \gamma + \alpha \boldsymbol{e}_j \left(\boldsymbol{e}_j^T \delta\boldsymbol{X}\right) \quad (18)$$

Then the following designations are introduced:

$$\boldsymbol{J}_\alpha \boldsymbol{d}_1 = -\boldsymbol{R} - \boldsymbol{e}_j \gamma \; ; \; \boldsymbol{J}_\alpha \boldsymbol{d}_2 = -\boldsymbol{R}_\lambda \; ; \; \boldsymbol{J}_\alpha \boldsymbol{d}_e = \alpha \boldsymbol{e}_j \; ; \; \beta_1 = \boldsymbol{e}_j^T \delta\boldsymbol{X} \quad (19)$$

and the increment of displacements takes the form:

$$\delta\boldsymbol{X} = \boldsymbol{d}_1 - \left(\boldsymbol{d}_e / \alpha\right)\delta\gamma + \delta\lambda \boldsymbol{d}_2 + \beta_1 \boldsymbol{d}_e \quad (20)$$

Substituting Eq.(20) in the second line of Eq.(16) we can obtain an expression for the increment of the null vector, $\delta\boldsymbol{h}$:

$$\delta\boldsymbol{h} = \boldsymbol{b}_1 + \boldsymbol{b}_2 \delta\lambda + \boldsymbol{b}_3 \beta_1 - \left(\boldsymbol{b}_3 / \alpha\right)\delta\gamma + \boldsymbol{d}_e \beta_2 \quad (21)$$

where

$$\boldsymbol{J}_\alpha \boldsymbol{b}_1 = -\boldsymbol{J}\boldsymbol{h} - \frac{\partial\left(\boldsymbol{J}\boldsymbol{h}\right)}{\partial\boldsymbol{X}}\boldsymbol{d}_1 \; ; \; \boldsymbol{J}_\alpha \boldsymbol{b}_2 = -\frac{\partial\left(\boldsymbol{J}\boldsymbol{h}\right)}{\partial\boldsymbol{X}}\boldsymbol{d}_2 - \frac{\partial\left(\boldsymbol{J}\boldsymbol{h}\right)}{\partial\lambda} \quad (22)$$

$$\boldsymbol{J}_\alpha \boldsymbol{b}_3 = -\frac{\partial\left(\boldsymbol{J}\boldsymbol{h}\right)}{\partial\boldsymbol{X}}\boldsymbol{d}_e \; ; \quad \beta_2 = \boldsymbol{e}_j^T \delta\boldsymbol{h} \quad (23)$$

Substituting Eq.(21) in third and fourth lines of Eq.(16) and in the last equation of Eq.(23) and, moreover, substituting Eq.(20) in the last equation of Eq.(19) we can obtain the following matrix equation with respect to 4 scalar unknowns, β_1, β_2, $\delta\lambda$ and $\delta\gamma$:

$$\begin{bmatrix} \boldsymbol{e}_j^T\boldsymbol{d}_e - 1 & 0 & \boldsymbol{e}_j^T\boldsymbol{d}_2 & -\boldsymbol{e}_j^T\boldsymbol{d}_e \\ \boldsymbol{e}_j^T\boldsymbol{b}_3 & \boldsymbol{e}_j^T\boldsymbol{d}_e - 1 & \boldsymbol{e}_j^T\boldsymbol{b}_2 & -\boldsymbol{e}_j^T\boldsymbol{b}_3 \\ \boldsymbol{h}^T\boldsymbol{b}_3 & \boldsymbol{h}^T\boldsymbol{d}_e & \boldsymbol{h}^T\boldsymbol{b}_2 & -\boldsymbol{h}^T\boldsymbol{b}_3 \\ \boldsymbol{R}_\lambda^T\boldsymbol{b}_3 & \boldsymbol{R}_\lambda^T\boldsymbol{d}_e & \boldsymbol{R}_\lambda^T\boldsymbol{b}_2 & -\boldsymbol{R}_\lambda^T\boldsymbol{b}_3 \end{bmatrix} \begin{Bmatrix} \beta_1 \\ \beta_2 \\ \delta\lambda \\ \delta\gamma/\alpha \end{Bmatrix} = -\begin{Bmatrix} \boldsymbol{e}_j^T\boldsymbol{d}_1 \\ \boldsymbol{e}_j^T\boldsymbol{b}_1 \\ 0.5r_2 + \boldsymbol{h}\boldsymbol{b}_1 \\ \boldsymbol{R}_\lambda^T\left(\boldsymbol{h} + \boldsymbol{b}_1\right) \end{Bmatrix} \quad (24)$$

Solution of this simple equation allows calculation of the increments for displacements and the null vector using Eqs.(20) and (21). It should be noted that such solution of the branching equation requires only one factorisation of the regularised Jacobian, $\boldsymbol{J}_\alpha$, and all the other operations are operations with scalars and vectors, which are not computationally expensive.

CALCULATION OF TANGENTS TO BRANCHING SOLUTIONS

When the bifurcation point is localised it is necessary to calculate tangents to all possible solutions emanating from this bifurcation point. Considering the displacements and the tracing parameters as functions of some arc-length coordinate, s, of the solution trajectory the tangent vectors are expressed:

$$\left\{\boldsymbol{t}_x, t_\lambda\right\}^T = \left\{\partial\boldsymbol{X}/\partial s, \partial\lambda/\partial s\right\}^T \quad (25)$$

For a regular point the tangent to the solution trajectory can be found from Eq.(10), obtained by taking first derivative of Eq.(4) with respect to s. For a bifurcation point this equation does not provide a unique tangent and it is necessary to use higher approximations for the solutions of Eq.(4). By taking second derivative of Eq.(4) with respect to s and multiplying it from the left by the null vector $\boldsymbol{h}^T$ calculated earlier we obtain:

$$\begin{aligned} \boldsymbol{h}^T \frac{\partial^2\boldsymbol{R}}{\partial s^2} &= \boldsymbol{h}^T \frac{\partial}{\partial s}\left(\frac{\partial\boldsymbol{R}}{\partial\boldsymbol{X}}\frac{\partial\boldsymbol{X}}{\partial s} + \frac{\partial\boldsymbol{R}}{\partial\lambda}\frac{\partial\lambda}{\partial s}\right) = \\ &= \boldsymbol{h}^T\left(\frac{\partial^2\boldsymbol{R}}{\partial\boldsymbol{X}^2}\boldsymbol{t}_x\boldsymbol{t}_x + 2\frac{\partial^2\boldsymbol{R}}{\partial\boldsymbol{X}\partial\lambda}\boldsymbol{t}_x t_\lambda + \frac{\partial^2\boldsymbol{R}}{\partial\lambda^2}t_\lambda^2\right) = 0 \end{aligned} \quad (26)$$

The trajectory tangents can be expressed as a linear combination of two known vectors, $\boldsymbol{h}$ and $\boldsymbol{h}_1$:

$$\left\{\boldsymbol{t}_x, t_\lambda\right\}^T = \left\{\zeta\boldsymbol{h} + \eta\boldsymbol{h}_1, \eta\right\}^T \quad (27)$$

where $\boldsymbol{h}_1 = \boldsymbol{d}_2 - \left(\boldsymbol{h}^T\boldsymbol{d}_2 / \boldsymbol{h}^T\boldsymbol{d}_e\right)\boldsymbol{d}_e$ and $\boldsymbol{h}$ is a vector calculated earlier. The substitution of Eq.(27) in Eq.(26) gives an equation with the respect to coefficients η and ζ:

$$a\zeta^2 + 2b\zeta\eta + c\eta^2 = 0 \quad (28)$$

where

$$a = \boldsymbol{h}^T\frac{\partial\left(\boldsymbol{J}\boldsymbol{h}\right)}{\partial\boldsymbol{X}}\boldsymbol{h}; \quad b = \boldsymbol{h}^T\left(\frac{\partial\left(\boldsymbol{J}\boldsymbol{h}\right)}{\partial\boldsymbol{X}}\boldsymbol{h}_1 + \frac{\partial\left(\boldsymbol{J}\boldsymbol{h}\right)}{\partial\lambda}\right) \quad (29)$$

$$c = \boldsymbol{h}^T\left(\frac{\partial\left(\boldsymbol{J}\boldsymbol{h}_1\right)}{\partial\boldsymbol{X}}\boldsymbol{h}_1 + 2\frac{\partial\left(\boldsymbol{J}\boldsymbol{h}_1\right)}{\partial\lambda} + \frac{\partial^2\boldsymbol{R}}{\partial\lambda^2}\right) \quad (30)$$

Eq.(28) can have two solutions at the most, which occur if $b^2 - ac > 0$ and this condition can be used to check whether the simple bifurcation point is calculated correctly. Moreover, there are the following possible cases for the solution depending on the value of coefficient, a:

1) a case of $a = 0$. This is the pitchfork bifurcation and two solutions of Eq.(28) are
   (i) $\eta = 0$; $\zeta = any$ and the corresponding tangent vector is
   $$\boldsymbol{t}_x = \boldsymbol{h}\,;\; t_\lambda = 0 \quad (31)$$
   (ii) $\eta/\zeta = b/\left(-c/2\right)$ and the tangent vector is
   $$\boldsymbol{t}_x = b\boldsymbol{h}_1 - 0.5c\boldsymbol{h}\,;\; t_\lambda = b \quad (32)$$
2) a case of $a \neq 0$. This is the asymmetric bifurcation and two solutions of Eq.(28) are
   (i) $\eta/\zeta = a/\left(-b - \sqrt{b^2 - ac}\right)$ and the tangent vector is
   $$\boldsymbol{t}_x = a\boldsymbol{h}_1 + \left(-b - \sqrt{b^2 - ac}\right)\boldsymbol{h}\,;\; t_\lambda = a \quad (33)$$
   (ii) $\eta/\zeta = a/\left(-b + \sqrt{b^2 - ac}\right)$ and the tangent vector is
   $$\boldsymbol{t}_x = a\boldsymbol{h}_1 + \left(-b + \sqrt{b^2 - ac}\right)\boldsymbol{h}\,;\; t_\lambda = a \quad (34)$$

It should be noted that all the tangent vectors (as also solutions for and η and ζ) can be multiplied by any nonzero coefficient and this coefficient can be used for the normalisation of the tangent vectors.

ALGORITHM OF TRACING NONLINEAR SOLUTIONS WITH BIFURCATIONS

The general procedure of the calculation of multiharmonic forced response is the following.

1) Tracing the solution trajectory using the standard solution continuation method with checking for each new found solution the sign of $\det\left(\boldsymbol{J}_1\right)$.

2) If this sign changes, which indicates the presence of the bifurcation, then the bifurcation point is localized by solution of the branching equation by Newton-Raphson method

3) For the found bifurcation point, two tangent vectors are calculated. These tangent vectors allow determination of good approximations for 4 solutions located on four branches emanating from the bifurcation point. These approximations are calculated for two different directions of each of two tangent vectors: multiplying the calculated tangents by positive and negative scaling coefficients. One of these 4 branches is a branch which have been already calculated, before we located the bifurcation point, and three others are new branches. To determine which of the found continuation directions are old and which are new, the scalar product of the tangent calculated at the last regular point of the solution trajectory, $\left(\boldsymbol{t}_x^*, t_\lambda^*\right)$ and the tangents calculated at a bifurcation point $\left(\boldsymbol{t}_x^j, t_\lambda^j\right)$, $j = 1..4$ are used. The smallest value of this product (which takes usually negative values) indicates that this tangent leads backwards, i.e. to the already calculated path and, therefore, this tangent is not used in the further analysis. The largest value usually indicates that this can be a continuation of the traced solution trajectory further, behind the bifurcation point and, therefore, this tangent is used to continue the solution tracing. Two intermediate values give new solution branches, and the corresponding two tangents are saved in a special file together with the bifurcation point parameters.

4) When solution tracing for the required range of parameter variation is finished for one branch, the solution tracing is then performed for each saved branching point and branching tangents separately. For each such tracing path new bifurcation points can be found and the algorithm given here in items 1) - 4) is applied recursively again.

ANALYTICAL EVALUATION OF MATRICES FOR BIFURCATION EQUATION

There is a significant number of matrices and vectors required to form and solve the branching equation and to calculate the branching solution tangents. There are two major requirements to allow robust and efficient calculation of forced response for structures with bifurcations: (i) these matrices have to be calculated with very high accuracy and (ii) these matrices have to be calculated fast. To meet these requirements all matrices involved in the bifurcation analysis are calculated analytically, for example:

$$\frac{\partial \boldsymbol{R}}{\partial \lambda} = \frac{\partial \boldsymbol{A}}{\partial \lambda}(\boldsymbol{F} - \boldsymbol{P}) + \boldsymbol{A}\left(\frac{\partial \boldsymbol{F}}{\partial \lambda} - \frac{\partial \boldsymbol{P}}{\partial \lambda}\right) \tag{35}$$

$$\frac{\partial^2 \boldsymbol{R}}{\partial \lambda^2} = \frac{\partial^2 \boldsymbol{A}}{\partial \lambda^2}(\boldsymbol{F} - \boldsymbol{P}) + 2\frac{\partial \boldsymbol{A}}{\partial \lambda}\frac{\partial (\boldsymbol{F} - \boldsymbol{P})}{\partial \lambda} + \boldsymbol{A}\frac{\partial^2 (\boldsymbol{F} - \boldsymbol{P})}{\partial \lambda^2} \tag{36}$$

$$\frac{\partial (\boldsymbol{Jh})}{\partial \boldsymbol{X}} = \boldsymbol{A}\frac{\partial (\boldsymbol{Kh})}{\partial \boldsymbol{X}} \tag{37}$$

$$\frac{\partial (\boldsymbol{Jh})}{\partial \lambda} = \frac{\partial \boldsymbol{A}}{\partial \lambda}(\boldsymbol{Kh}) + \boldsymbol{A}\frac{\partial (\boldsymbol{Kh})}{\partial \lambda} \tag{38}$$

The analytical expressions for first and second derivatives of the FRF matrix $\boldsymbol{A}$ of the linear structure with respect to modal properties (i.e. modal damping factors and natural frequencies) and with respect to the principal excitation frequency can be easily calculated, as shown in Ref.[22]. The vector of multiharmonic nonlinear forces, $\boldsymbol{F}$ and the nonlinear tangent stiffness matrix, $\boldsymbol{K}$, together with their different derivatives in Eqs.(35)-(38) are calculated by summation of such derivatives obtained separately for each of the multitude contact interface elements describing the nonlinear contact interactions. The library of the contact interface elements includes gap, friction contact, cubic nonlinearity and rotor-stator rubbing contacts. Derivation of some expressions for these elements can be found in Refs.[11]-[13] and [23]. In order to calculate matrices which are specific for the bifurcation analysis, such as $\partial(\boldsymbol{Kh})/\partial \boldsymbol{X}$ and $\partial(\boldsymbol{Kh})/\partial\lambda$ a special facility has been added for each of these contact interface elements. The derivation of these terms takes into account the fact that the tangent stiffness matrix, $\boldsymbol{K}$, is dependent on λ and $\boldsymbol{X}$ but $\boldsymbol{h}$ is constant vector which is independent from those variables .

NUMERICAL EXAMPLES

The methodology developed here has been introduced in a computer code which demonstrated its efficiency in all cases analysed by the author. Some of examples of analysis of structures having the bifurcations are given below.

A simple model with cubic nonlinearity

First example is a one-degree of freedom model of a rotor described by the Duffing equation:

$$m\ddot{x} + c\dot{x} - k_1 x + k_3 x^3 = F_0 \sin \omega t \tag{39}$$

The following parameters of the model given by equation are chosen for numerical studies: F_0=2000N; m=1kg; c=1Ns/m; k_1=1000N/m k_3=10000 N/m^3. This equation was used in Ref.[24] for modelling a rotor test rig shown in **Fig. 2** where one of the rotor supports is designed from a couple of thin plates to model stiffness properties of magnetic bearings.

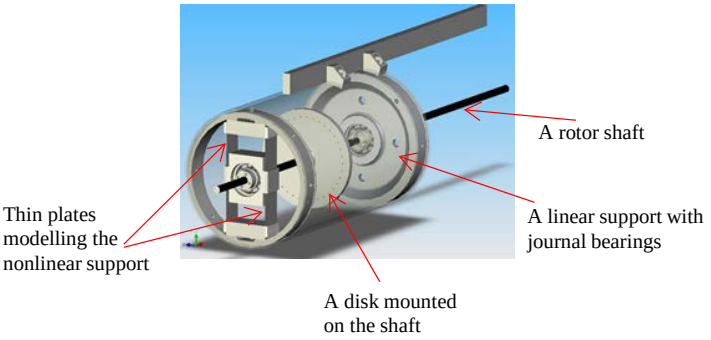

Fig. 2 A rotor with negative linear stiffness

The plates are compressed and the pre-stressed plate state provides the negative linear stiffness coefficient and positive cubic stiffness coefficient. It should be noted that such plates have three static equilibrium positions, shown in **Fig. 3**: (i) straight plate (unstable equilibrium); (ii) plate bent on the left and (iii) the plate bent on the right.

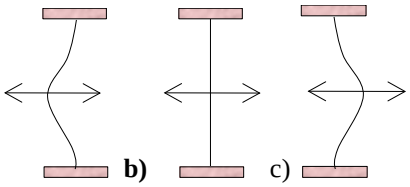

Fig. 3 Equilibrium configurations for the pre-stressed rotor support

The forced response of this model is performed by keeping first all 20 harmonics: from 0 to 19 and assuming that the excitation frequency varies within the frequency range from 1 to 30 Hz. The maximum displacement values obtained by tracing the major solution branch are plotted in **Fig. 4** and circles indicate the found bifurcation points.

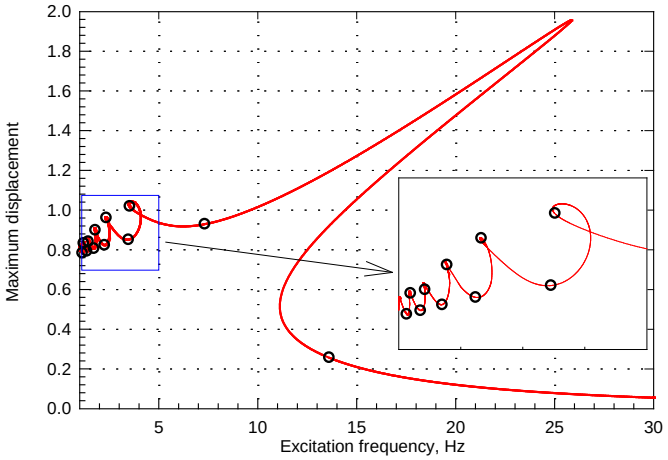

Fig. 4 Forced response of a simple rotor model: major solution curve and bifurcation points

It should be noted that this solution curve corresponds to solutions with zero and even harmonic coefficients in the multiharmonic expansion equal to zero. Therefore, this curve can be calculated by keeping only odd harmonics in the multiharmonic representation of displacements. Determination of the bifurcation point at frequency 13.6 Hz requires inclusion of zero harmonic in the multiharmonic expansion although even harmonics still can be omitted. To find all bifurcation points in the low frequency range from 1 to 8 Hz (where multitude of superharmonic resonance peaks is observed), even harmonics have to be included in the analysis.

All forced response solutions for including the branching solutions emanating from the bifurcation points are plotted in **Fig. 5**. Since the equilibrium state changes for the structure analysed the maximum (positive) and minimum (negative) displacement values can differ and both these values are drawn in this plot. Solution corresponding to same solution branches are plotted in the same colour: red, green or blue. One can see that at the bifurcation point 13.6 Hz two new stable solutions occur. These solutions correspond to vibrations with respect to the left bent equilibrium (blue lines) and right bent equilibrium (green lines) and the constant term in the multiharmonic displacement representation become significant and, for higher frequencies, even dominant.

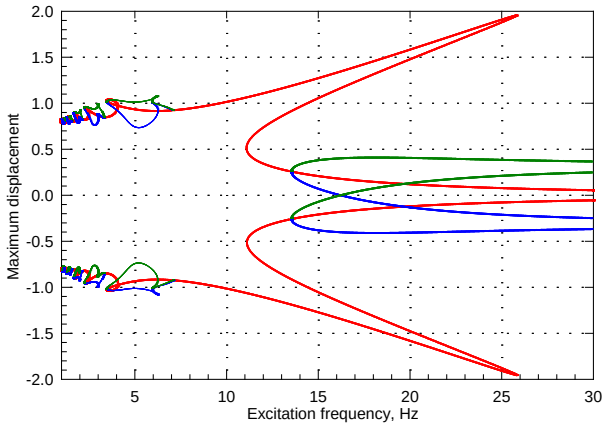

Fig. 5 Forced response of a simple rotor model with all found bifurcation branches

The solution branch of vibrations with the equilibrium corresponding to straight plate becomes unstable. The stability analysis was based on the Floquet theory (e.g. see Refs. [25] and [26]). The amplitudes of bifurcation branches for superharmonic vibrations observed for lower frequencies differ from the major solution relatively little. In order to show the shapes of the bifurcation solution in detail, their zoomed view is given in **Fig. 6**. It is interesting that all found bifurcation solutions form closed loops and they starts at one bifurcation point and finish and the following bifurcation point.

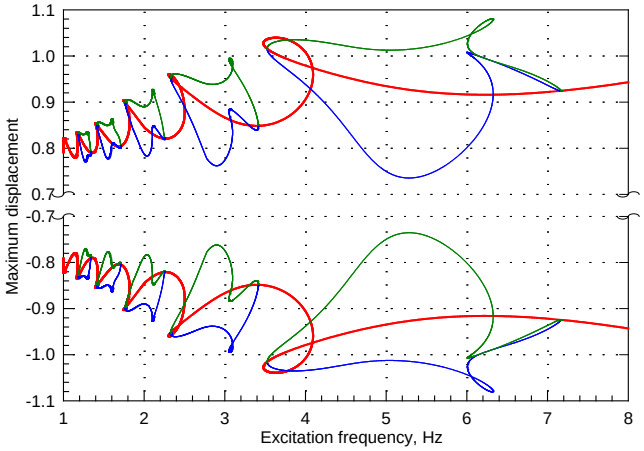

Fig. 6 Forced response of a simple rotor model with all found bifurcation branches: a zoomed view for a low-frequency range

Comparison of results of the developed method for frequency domain multiharmonic bifurcation analysis and the results obtained by integration of the equation of motion Eq.(39) are shown in **Fig. 7** and **Fig. 8**. For the time domain analysis it is assumed that the excitation frequency is varied linearly: the excitation frequency is increased for **Fig. 7** and it is decreased for **Fig. 8**.

The rate of frequency variation for the time-domain analysis is set to be small enough to ensure that transient processes would not affect the response significantly and the obtained results are close to the steady-state vibrations. The rate of frequency variation is chosen here to be 3.0e-2 sec^{-2}. The time domain solutions are plotted in these figures in black and due to large number of plotted cycles they merge and seen in the plots as black areas. One can see a good correspondence between results obtained by the two approaches and abrupt changes of the levels of vibration amplitudes while passing the limit points.

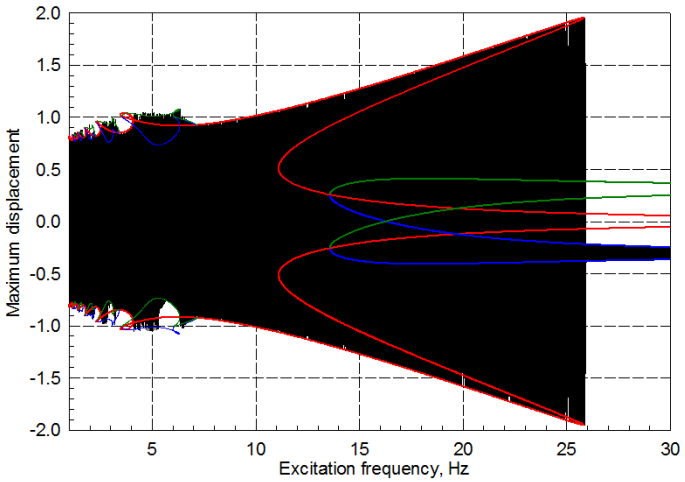

Fig. 7 Comparison of time domain (black line) and frequency domain solutions (colour lines): a case of frequency increasing

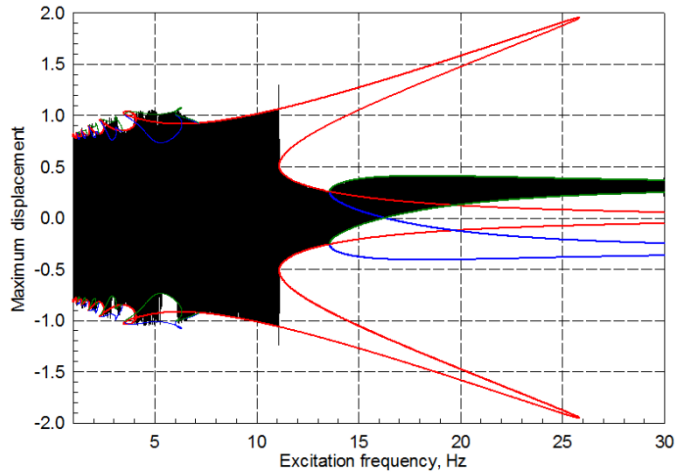

Fig. 8 Comparison of time domain (black line) and frequency domain solutions (colour lines): a case of frequency decreasing

A gas-turbine engine model

The properties of the method developed have been also explored on the example of a whole engine model to demonstrate the method efficiency in application to typical large size models. The model comprises more than 1300 DOFs, which is still small enough to allow the time domain integration of the equations of motion. Four nonlinear snubbing contacts describing rotor-stator rubbing interactions are allowed for in the model: including fan-casing interactions, rubbing contact in compressor and bearings. The rubbing contact interaction model include gap nonlinearity and friction force occurring as a result of interaction of the rotating rotor components with stator. Detailed description of the contact elements used for modelling of such interactions can be found in Ref.[23]. The major objective here is to study the forced response in the event of nonlinearities due to rotor casing rubs, e.g. following damage to the rotor blading and other unbalances in the whole engine model. In order to achieve this some model parameters such as levels of unbalance, bearing support flexibilities, etc. were altered to show up the non-linear effects. The forced response analysis was performed for this model, before the bifurcation method has been developed and implemented (see Ref.[23]). For the analysis only odd harmonics from range 0 to 11 were included initially in the multiharmonic displacement representation. The results were compared with the time domain solutions. The displacements were calculated at some critical locations and the good correspondence between time and frequency domain solutions was achieved (**Fig. 9**). However, for some regimes, comparison of contact interface forces indicated significant differences in the results for some narrow, but nevertheless practically important rotation frequency ranges. After the addition of even harmonics the solution tracing process had started to experience problems in the continuation at some frequencies which are indicated in **Fig. 9** by red vertical lines and these frequencies correspond to the bifurcation points.

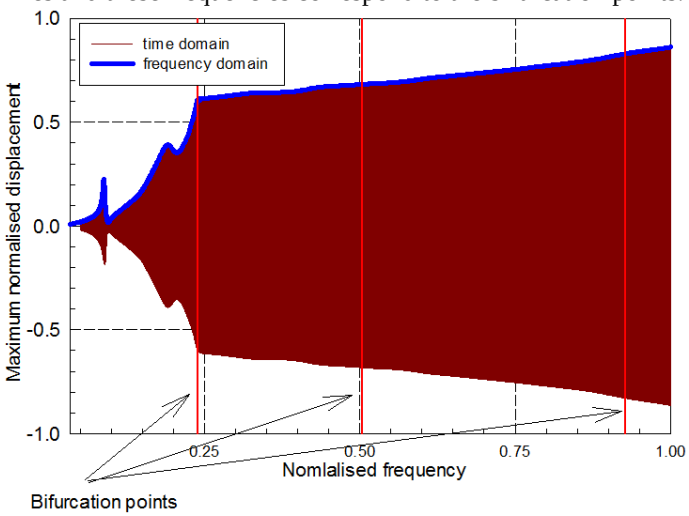

Fig. 9. Time domain (dark red line) and frequency domain solutions (blue line): the difference between displacements of bladed disc and casing

The new method has allowed the determination of all these bifurcation points and the calculation of all branching solutions. The results of calculation by the method developed are shown in **Fig. 10** - **Fig. 13**. To illustrate the branching trajectories more clear the variation of the contact interaction forces is plotted here instead of displacements. Three of the four rotor-stator rubbing contacts are selected: where the effects of the bifurcations are more prominent. In **Fig. 10** the contact force at 3rd rubbing contact are shown. One can see that two bifurcation regions can

be observed here: (i) in the vicinity of normalised frequency 0.24 and (ii) in the vicinity of normalised frequency 0.93. The bifurcation in the vicinity of frequency 0.5 is not visible here. The bifurcations in vicinity of frequency 0.24 occur when the rotor comes in contact with the stator first time during the acceleration process. The bifurcation curves are small here and they are shown in **Fig. 11** in a zoomed view. One can see that, similar to the case of the simple rotor, the solution branches form here a closed loop and two bifurcation points are located here at normalised frequency values: 0.2384 and 0.2387.

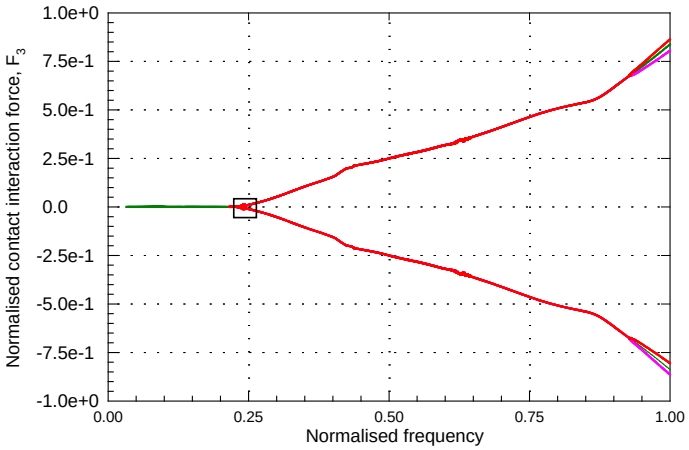

Fig. 10. Contact interaction force at 3rd rubbing contact for all branching solutions

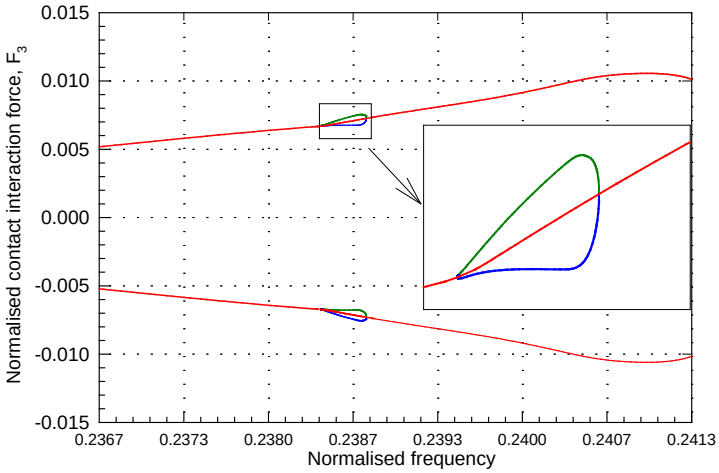

Fig. 11. Contact interaction force at 3rd rubbing contact for all branching solutions: a zoomed view

The contact interaction force at the rubbing contact 1 is plotted in **Fig. 12**. One can see that the bifurcations occur here when the rotor comes into contact with a casing at this location. There are four closely-spaced bifurcation points at normalised frequency values: 0.5056, 5068, 5069 and 5071. Moreover, the different bifurcation branches for the bifurcation point in vicinity of frequency 0.93 are observed here clearly.

The contact interaction forces at 4th rotor-casing contact point are shown in **Fig. 13** where one can see the bifurcation branches occurring at normalised frequency 0.93. Only solutions emanating from this bifurcation point is observed here since the rotor and stator do not come into contact at this location for all other bifurcations shown above.

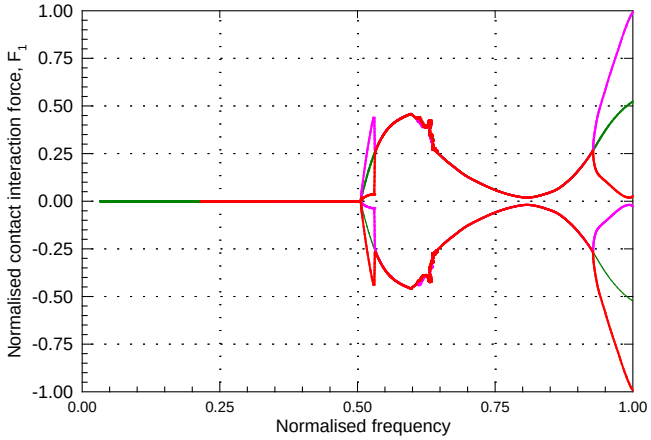

Fig. 12. Contact interaction force at 1st rubbing contact for all branching solutions

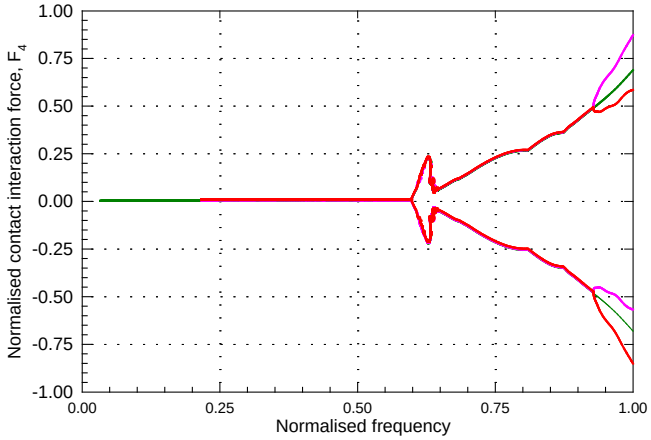

Fig. 13. Contact interaction force at 4th rubbing contact for all branching solutions

The comparison of time domain solutions and the results obtained by the developed method are shown in **Fig. 14** - **Fig. 16** on the example of the rubbing contact forces at 1st contact location. Here, we can observe that the time domain solutions can follow different solution branches at the bifurcation points. In **Fig. 14** and **Fig. 15** the time domain results are obtained for the rotor acceleration when the excitation frequency and the unbalance forces are increasing. One can see that the time domain solutions differ at normalised frequency value 0.5 and we have two different cases, although they follow the same path at the bifurcation frequency 0.93. This effect was achieved by a choice of different initial condition and small change of the rate of rotation speed increase.

A case of rotor deceleration is considered in **Fig. 16**. For this case the structure follows the solution branch different from 1st acceleration case for higher frequencies and for frequencies smaller 0.93 it behaves similar to the case 2 of the accelerating rotor. In all cases analysed, including shown here, the correspondence with the results obtained by the time and the developed method is very good.

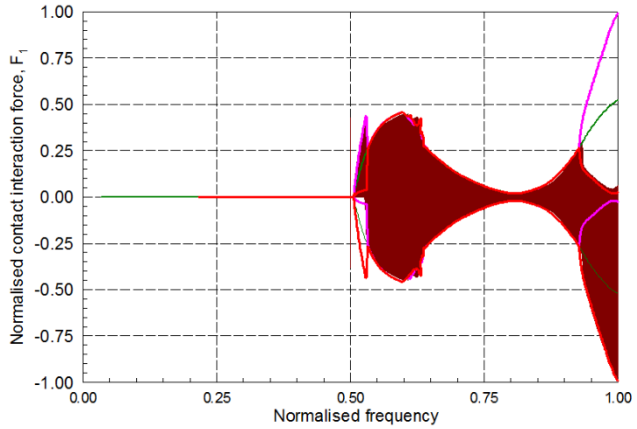

Fig. 14. Time and frequency domain solutions: contact force at 1st rubbing contact for rotor acceleration, case 1

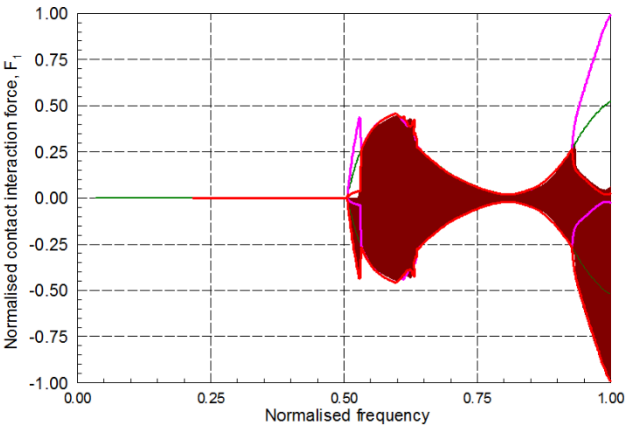

Fig. 15. Time and frequency domain solutions: contact force at 1st rubbing contact for rotor acceleration, case 2

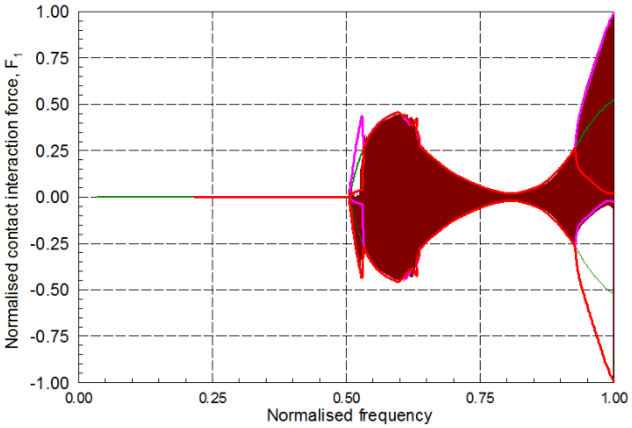

Fig. 16. Time and frequency domain solutions: contact force at 1st rubbing contact for rotor deceleration

On the classification of the found bifurcation points

The analysis of coefficients of Eq.(28) calculated at a bifurcation point can help to distinguish between two major types of the bifurcations considered here: (i) a pitchfork bifurcation and (ii) an asymmetric bifurcation. The condition for the pitchfork bifurcation is: $a = 0$, but in practical calculations, due to inherent numerical inaccuracies, this condition was never satisfied exactly. Hence, the comparison of the relative magnitudes of coefficients a, b and c are used for the identification of the bifurcation type. The relative coefficient values are plotted in Fig. 17 for all 12 bifurcation points found for the simple rotor and for 7 bifurcation points found for the gas-turbine engine model. The bifurcation points are counted here from low frequency to higher frequency values. One can see that all bifurcations of the simple rotor model can be attributed to the pitchfork type, although for lower frequency bifurcation points (corresponding to vibrations with significant contributions of higher harmonics to the forced response), the bifurcations deviate slightly from the pitchfork type. For the whole engine model two first bifurcations (in the vicinity of the frequency 0.24) are pitchfork bifurcations and all the other are asymmetric bifurcations.

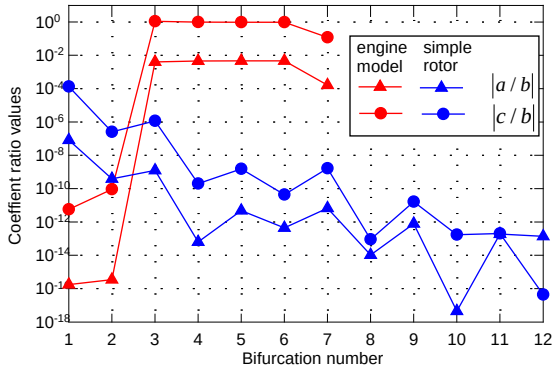

Fig. 17. Relative coefficient values of the tangents' equation

Numerical efficiency of the method

Before illustrating the numerical efficiency of the method developed here we should note the following important facts.

1) In most cases the solution tracing, performed for a nonlinear structure with solution bifurcations, becomes very difficult without the special treatment of the bifurcation points: since the usual tracing algorithms cannot progress along the solution trajectory and make usually infinite loops in the vicinity of the bifurcation points. The tracing process has to be stopped manually at each bifurcation point and, for a case when the solution has to be found over the whole parameter variation range, an exclusion of all bifurcations points is needed. Moreover, the determination of a good approximation for a solution after the excluded bifurcation point, which is necessary for the solution continuation, is very problematic in many cases.

2) The exclusion of some selected harmonics from the multiharmonic representation of the forced response may help to avoid occurring the solution bifurcations and, therefore, allows, sometimes, the calculation of a solution which can be sufficiently close to the vibration regime occurring in an actual structure. Nevertheless, such approach not only fails to determine the possible bifurcation solution branches, but also the accuracy of the found solution becomes questionable.

3) The extended Jacobian determinant used for the detection of the bifurcation points using Eq.(14) is obtained as a by-product of the solution process and does not require significant additional computations.
4) The solution continuation process over a range of tracing parameter variation involves usually calculation of several hundred or more solution points located on a selected trajectory of solutions. The number of bifurcation points is usually small: e.g. for the simple rotor model there are 12 bifurcation points and for the whole engine model the number of bifurcations is 7 in the considered frequency range.
5) The calculation of an accurate bifurcation point location is the most time consuming part in the bifurcation analysis. Nevertheless, the computational effort required for localisation of the bifurcation points using Eqs.(15)-(24) together with the calculation of the tangents to the solution trajectory is comparable with the effort needed to calculate a single solution in the solution continuation process.
6) The matrices and vectors involved in these calculations are obtained analytically which provides high speed and accuracy of calculation for these matrices. The convergence of the bifurcation localisation in the vicinity of the bifurcation points is in many cases close to quadratic, as it can be achieved for Newton-Raphson iterative solution with accurate Jacobian.

The time of forced response calculations for both structures considered in this paper are given in **Table 1**. The calculations are compared here for cases when the bifurcation analysis (BA) is performed and when it is switched off. Moreover, the times of calculation using the time-marching method are provided.

Table 1. Computational time of the forced response analysis

Structure	Simple rotor		Engine model	
Harmonics included	odd harmonics	all from 0 to 18	odd harmonics	all from 0 to 11
Without BA	18.84 sec	n/a	273.99 sec	n/a
With BA	19.81 sec	43.62 sec	278.56 sec	535.61 sec
Time domain analysis	78.6 sec		31344 sec	

When only odd harmonics are included, the analysis without BA can be performed over the whole frequency range considered, since the equations do not have bifurcations. The analysis with BA involves the calculation of the determinant for the extended Jacobian and it is evident that the time increase is negligibly small. When odd and even harmonics are included, the analysis cannot be performed for the whole frequency range without BA and the BA computational time is provided here only. This time is given for the same solution branch which is traced when only odd harmonics are kept. The analysis with BA includes here all components of the developed method: detection and localization of all bifurcations, calculation of tangents to the solution trajectory at the bifurcation points, and calculation of starting points for all branching solution trajectories. Comparing computation times of BA analyses for two cases: (i) with odd harmonics and (ii) with all harmonics included, one can see that the calculation times increase by factor of two and this increase should be attributed mostly to the increase of the size of nonlinear equations when the number of harmonic doubles.

The convergence of the solution of Eq.(15) can represent a serious problem, if its Jacobian is not evaluated accurately and the initial solution approximation is not close enough to the solution. The proposed numerical procedure provides robust and quickly converged solutions, which is illustrated in Fig. 18 and Fig. 19 for both considered structures and for all detected bifurcation points. The values of the Jacobian determinant for each iteration in the process of bifurcation localisation are plotted here. One can see that for all bifurcation points the number of iterations from 4 to 9 can lead to the decrease of the Jacobian determinant by 10-12 orders of magnitude and, therefore, provide sufficient accuracy for the bifurcation point determination.

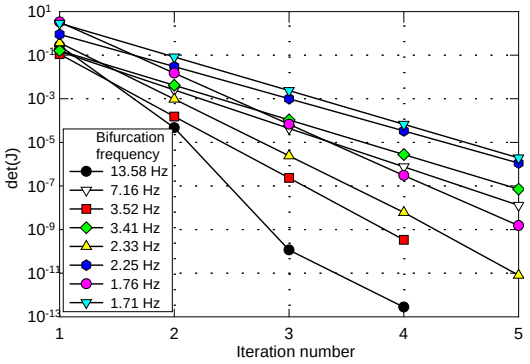

Fig. 18 Convergence of the bifurcation localisation: the simple rotor case

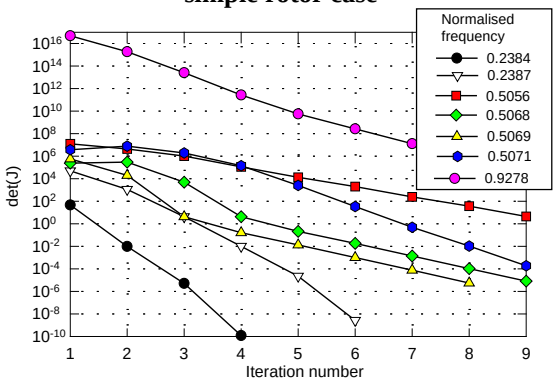

Fig. 19 Convergence of the bifurcation localisation: the gas-turbine engine model

CONCLUSIONS

An efficient frequency-domain method has been developed to analyse the forced response of large-scale nonlinear gas-turbine structures with bifurcations.

The method allows: (i) detection and (ii) localization of the design and operating conditions sets where bifurcations occur; (iii) calculation of tangents to the solution trajectory and (iv) continuation of solutions under parameter variation for structures with bifurcations.

The method is aimed at calculation of steady-state periodic solution and multiharmonic representation of the variation of displacements in time is used. The method can calculate

bifurcation regimes for major, subharmonic and superharmonic vibrations.

All equations required for dealing with the bifurcation points and solution branches are derived analytically which, together with new special facilities for the multiharmonic contact interface elements, provide the means for fast and highly accurate analysis.

The excellent numerical properties and accuracy of the method are demonstrated on a simple rotor model and on a large rotor-casing model.

The possibility of bifurcations in realistic structures with friction contacts and with cubic nonlinearity has been discovered. It was found that, in most of the considered cases, the bifurcation branches formed closed loops.

ACKNOWLEDGEMENTS

The author is grateful to Rolls-Royce plc. for providing the financial support for this work and for giving permission to publish this work. He is also grateful to his colleague at the Vibration UTC, Imperial College, Prof. D.J.Ewins for useful discussions.

REFERENCES

[1] Sanliturk, K.Y., Imregun, M., and Ewins, D.J., 1997, "Harmonic balance vibration analysis of turbine blades with friction dampers," *Trans. ASME: J. of Vibration and Acoustics*, Vol. 119, pp. 96-103

[2] Chen, J., Menq, C., 2001, "Prediction of periodic response of blades having 3D nonlinear shroud constraints," *J. of Eng. for Gas Turbines and Power*, Vol. 123, pp. 901-909.

[3] Petrov, E.P., Ewins, D.J., 2003, "Analytical formulation of friction interface elements for analysis of nonlinear multi-harmonic vibrations of bladed discs", *ASME J. of Turbomachinery*, Vol.125, pp.364-371

[4] Zucca, S., C.M. Firrone, and M.M. Gola, (2012). Numerical assessment of friction damping at turbine blade root joints by simultaneous calculation of the static and dynamic contact loads. *Nonlinear Dynamics*, 67(3): p. 1943-1955.

[5] Laborenz, J., M. Krack, et al. (2012). "Eddy Current Damper for Turbine Blading: Electromagnetic Finite Element Analysis and Measurement Results." *J. of Eng. for Gas Turbines and Power*, 134(4).

[6] Siewert, C., et al. (2009), "Multiharmonic forced response analysis of a turbine blading coupled by nonlinear contact forces", *Proc. of ASME Turbo Expo, Florida, USA*, GT2009-59201

[7] Batailly, A., M. Legrand, et al. (2012). "Numerical-experimental comparison in the simulation of rotor/stator interaction through blade-tip/abradable coating contact." *J. of Eng. for Gas Turbines and Power*, 134(8).

[8] E. Cigeroglu, N. A. and C-H. Menq, (2007), "Wedge damper modeling and forced response prediction of frictionally constrained blades", *Proc. of ASME Turbo Expo*, Montreal, Canada, GT2007-27963

[9] Cameron, T.M. and Griffin, J.H. (1989) "An alternating frequency/time domain method for calculating steady response of nonlinear dynamic systems", *Trans. of ASME: J. of Applied Mechanics*, Vol. 56, pp.149-154

[10] Cardona, A., Coune, T., Lerusse, A, and Geradin, M. (1994) "A multiharmonic method for non-linear vibration analysis," *Int. J. Numer. Meth. Eng*., Vol. 37, pp. 1593-1608

[11] Petrov, E.P., 2007, "Direct parametric analysis of resonance regimes for nonlinear vibrations of bladed discs", *Trans. ASME: J. of Turbomachinery*, Vol.129, pp.495-502

[12] Petrov, E.P, 2009, "Method for sensitivity analysis of resonance forced response of bladed disks with nonlinear contact interfaces", *Trans. ASME: J. of Eng. for Gas Turbines and Power*, Vol.131, July, pp.022510-1-022510-9

[13] Petrov, E.P., (2005),"Sensitivity analysis of nonlinear forced response for bladed discs with friction contact interfaces", *Proc. of ASME Turbo Expo*, Reno-Tahoe, USA, GT2005-68935, 12pp

[14] Kuznetsov, Y. A. (1998) "Elements of Applied Bifurcation Theory", Springer-Verlag, New York

[15] G. Moore and A. Spence. (1980) "The calculation of turning points of nonlinear equations," *SIAM Journal on Numerical Analysis*, Vol. 17, No. 4, pp. 567-576

[16] Geradin M and Cardona A. (2001) "Flexible Multibody Dynamics: A Finite Element Approach", John Willey & Sons Ltd., 327 pp.

[17] Felippa, C. A., (1987) Traversing critical points by penalty springs, *Proceedings of NUMETA'87 Conference*, Swansea, Wales, Nijhoff Pubs, Dordrecht, Holland, pp. C2/1-C2/8

[18] Wriggers, P; Simo, J.C. (1990) "A general procedure for the direct computation of turning and bifurcation points", *Int. J. for Num. Methods in Engineering*, Vol. 30, pp. 155-176

[19] Riks, E., (1979), "An incremental approach to the solution of the snapping and buckling problems," *Int. J. Solids Struct*., 15, pp. 529–551.

[20] Crisfield, M., (1981), "A fast incremental/iterative solution procedure that handles snap-through," *Comput. Struct.*, 13, pp. 55–62.

[21] Fried, I., 1984, "Orthogonal trajectory accession to the nonlinear equilibrium curve," *Comput. Methods Appl. Mech. Eng*., 47, pp. 283–297.

[22] Petrov, E.P., 2014,"Sensitivity analysis of multiharmonic self-excited limit-cycle vibrations in gas-turbine engine structures with nonlinear contact interfaces", *Proc. of ASME Turbo Expo*, June 16 – 20, Germany, GT2014-26673

[23] E.P. Petrov, "Mutliharmonic analysis of nonlinear whole engine dynamics with bladed disc-casing rubbing contacts", *Proc. of ASME Turbo Expo 2012*, June 11-15, 2012, Copenhagen, Denmark, GT2012-68474

[24] Huang, S., Petrov, E.P. and Ewins, D.J. (2006) "Comprehensive analysis of periodic regimes of forced vibration for structures with nonlinear snap-through springs" *Proc. of 6th Int. Conf. on Modern Practice in Stress and Vibr. Analysis*, Bath, UK, pp. 443-453

[25] J. DaCunha, J. Davis, (2011) "A unified Floquet theory for discrete, continuous, and hybrid periodic linear systems", *J. of Diff. Equations*, Vol. 251, No. 11, pp. 2987-3027

[26] Von Groll, G. Ewins, D.J. (2001) "The harmonic balance method with arc-length continuation in rotor/stator contact problems", *J. of Sound and Vibration*, v 241, n 2, p 223-233

